УДК 544.252

Liquid Crystalline Polymers: Theories, Experiments and Nematodynamic Simulations of Shearing Flows

Hongyan Chen, **Leonov A.I.** leonov@uakron.edu

Department of Polymer Engineering, The University of Akron
Akron, Ohio 44325-0301

Processing of bioorganic foods (biopolymers) must be done based on the properties containing them lyotropic liquid crystals. More than thirty years of research on liquid crystalline polymers (LCP) resulted in a huge amount of publications on physics, constitutive modeling and experimental results, which are briefly reviewed in this article. To date, some theories have been experimentally verified but only for steady simple shearing cases. Thus the simulations shown in this article present the first attempt to describe the unsteady shearing rheological properties of LCP and more specifically, thermotropic type of LCP where till recently no constitutive modeling was known. Recently developed monodomain thermodynamic theory of weakly viscoelastic nematodynamics has been employed for simulations. Our simulations of steady and start up shearing flows with relaxation demonstrate at least a semi-quantitative agreement with experimental data for two industrial and two model LCP, although the model LCP exhibit the polydomain features. Established dependencies of fitted theoretical parameters on temperature and structure of LCP have also been discussed.
Keywords: liquid crystal polymers, nematodynamics, viscoelasticity

---

Жидкокристаллические полимеры : теория , эксперименты и моделирование нематодинамического сдвигового течения

Хонгян Чен, **Леонов А.И.** leonov@uakron.edu

Департамент Полимерное машиностроение ,Университет Акрона
Акрон, штат Огайо 44325-0301 , США

Переработка биоорганических пищевых продуктов (биополимеров) должна производится с учетом свойств содержащих в них лиотропных жидких кристаллов. Более тридцати лет исследований жидкокристаллических полимеров (ЖКП), привели к огромному количеству публикаций по физике , моделированию и экспериментальным результатам, которые кратко рассматриваются в этой статье. На сегодняшний день некоторые теории нашли экспериментальное подтверждение, но только для простых случаев стационарного сдвига. Таким образом, моделирование в этой статье представляет первую попытку описать нестационарные сдвиговые реологических свойств ЖКП и , более конкретно , термотропный типа ЖКП , где до последнего времени адекватное моделирования не было известно. В последнее время разработанная монодоменная термодинамическая теория слабой нематодинамической вязкоупругости была здесь использована для моделирования. Наше моделирование устойчивого и стартового сдвигового потоков с релаксацией продемонстрировать, по крайней мере, в полу-количественном согласии с экспериментальными данными для двух промышленных и двух модельных ЖКП , хотя модель ЖКП проявляют полидоменные особенности. Основанная зависимости теоретических параметров от температуры и структуры ЖКП также обсуждались.

Ключевые слова: жидкокристаллические полимеры, нематодинамика, вязкоупругость

1. Introduction and Review

1.1. Low Molecular Weight and Polymeric Liquid Crystals

Low molecular weight liquid crystals (LC) have found large applications in many industries, especially in electronics. LC display very specific properties characterizing by such solid like effects as orientation of large group molecules under physical or stress fields coupled with flow [1-5]. Internal rotations, a specific Frank elasticity caused by mutual rotations of molecules, and anisotropic flows are common effects established for this type of liquids. Molecules in LC are arranged in an orderly manner, and there are three different types of their ordered structure, nematic, cholesteric, and smectic. The nematic structure where the molecules have a long-range orientation order but only a short-range positional order can be met more often, because it has low ordered structure as compared to other LC types. Remarkable, continuum type theories are the most common for description of both the elastic and viscous LC properties. They are: Frank theory for LC elasticity and Leslie-Ericksen-Parody (LEP) for viscous properties of LC.

The quest for lightweight materials with great strength and stiffness has led to the synthesis of liquid crystalline polymers (LCP) and occurrence of novel processes and theories to predict and control the LCP structures in final products. In LCP, the liquid crystalline properties are achieved either by insertion of rigid chemical fragments either into the main polymer chain (main chain LCP) or by creating side branches (side chain LCP). To date, liquid crystalline polymers have found a variety of applications such as high-strength plastic fibers, bullet-proof garments, front panels of computers, cellular phones, electronic diaries, portable televisions, printed circuit boards, etc [6]. Typically LCP's have outstanding mechanical properties at high temperatures, excellent chemical resistance, inherent flame retardancy, heat aging resistance, low viscosity, and good weather resistance. It makes LCP's ideal candidates for high-performance applications [7].

Similarly to the low molecular weight LC, specific polymers display LC properties in a certain intermediate state between the solids and liquids, which is called mesophase, with the combined properties of both the crystalline and liquid states [5-7]. The molecular orientation order of chemical rigid fragments makes a polymeric material anisotropic and "crystalline", while the lack of strong positional order allows the material to flow like ordinary fluids. LCP's whose phase transition into the liquid crystalline phase occurs under change in temperature are called *thermotropic*, while a variety of LCP's which exhibit phase transitions by changing the polymer concentration in a solvent (as well as temperature) are called *lyotropic* liquid crystals. The unique feature of mesophase is that it is described by a positional order parameter, because it is geometrically anisotropic in space. Currently, the polymer nematics include liquid crystalline polymers and liquid crystalline elastomers (LCE) [3]. Similarly to LC, the action of external field or flow causes the orientation of mesogens of LCP or LCE, which induces uniaxial anisotropy, with an additional degree of freedom - internal rotations. In certain cases, LCP's or LCE's possess partial flexibility, which displays macroscopically as common anisotropic molecular elasticity or viscoelasticity, and thus is important for dynamics of these systems.

1.2. Molecular and Continuum Theories of LCP

Theoretical and experimental studies of nematic materials, extensively published during many years, produced enormous amount of publications. Luckily, several excellent texts (e.g. see [1-5]) are now available. These texts present in historical perspective a balanced view of the most important experimental effects and their theoretical explanations, both of continuum and molecular types.

Two types of theories, continuum and molecular, attacked the problem of modeling nematodynamic properties of LCP and LCE. The continuum theories try to establish a general framework with minimum assumptions of molecular structures, involving, however, many material parameters related to both the basic properties of symmetry and interactions described by the state variables. On the contrary, the molecular approaches employ many particular assumptions and describe the LCP properties with few molecular parameters. De Gennes [8] was seemingly first attempted to extend the LEP theory to nonlinear case. Doi characterized this attempt as following [9]: "A way of generalizing the Ericksen-Leslie theory to the nonlinear regimes was suggested by de Gennes [8]. However, this phenomenological approach has not been pursued very far since the number of unknown parameters increases as more complexity is introduced. In this paper, I describe a complementary approach, the molecular theory. Since this approach is based on a specific modeling of a system, it is less general, but it can give explicit results for rheological functions". Hopefully, the phenomenological and molecular theories will not be contradictory but supplemental.

De Gennes and Prost [2] first developed the concept of *nematodynamics*. It was defined as a set of problems for deformation and flow of the nematic systems under stress and external (magnetic and/or electrical) fields that can be solved or analyzed using specific macroscopic field equations. The research on polymer nematics has attracted long-standing academic and industrial interests for about three decades. Yet only few LCP have been in practical use, which is mostly due to the lack of knowledge of the complicated behavior of these systems. Therefore, nematodynamic studies are imperative for stimulating the progress in processing of polymer nematics and predicting the properties of post-processed products.

Larson and Mead [10] extended the Ericksen LC phenomenology to viscoelastic case, using instead of Ericksen's viscosities some linear viscoelastic memory functionals. Because these functionals were unknown, Larson and Mead exemplified their approach employing the linearized Doi theory [9, 11]. Using symmetry arguments, Volkov and Kulichikhin [12] proposed a continuum but non-thermodynamics approach to weak anisotropic viscoelasticity of Maxwell type with internal rotations. Pleiner and Brand [13, 14] developed a thermodynamic theory for linear anisotropic viscoelasticity of LCP, using along with state variables also their space gradients. However, the experience accumulated in many applications of continuum non-equilibrium thermodynamics clearly indicates that except for very specific cases, extending the set of state variables with the use of their time-space derivatives leads to an awkward description, which typically involves a huge amount of material parameters without recommending how to fit them to experimental data. Rey [15, 16] applied a very particular thermodynamic approach to weak viscoelasticity of LCP but obtained doubtful results of asymmetric stress. Terentjev and Warner [3, 17] developed a thermodynamic theory of solid viscoelasticity for LC elastomers, based on the Kelvin-Voigt type of nematic modeling (see also Fradkin *et al* [18]). Leonov and Volkov [19-21] initiated thermodynamic studies of nonlinear nematic viscoelasticity for various polymer systems of different rigidity, such as LCP, LCE and precursors of polymer nanocomposites. These approaches have met mathematical difficulties mentioned by Doi [9] and were overcome with creating a new mathematical tool, algebra of nematic operators [22]. Based on this tool a new nematodynamic theory [23] of LCP has been formulated.

A lot of theoretical effort was also undertaken to develop molecular theories that could model the lyotropic LCP, starting from Doi theory [9, 11]. Marrucci and Greco [24], Larson and co-authors (see references in the text

[5]), and Feng *et al* [25] typically use and elaborate the Doi's long rigid rod approach. Edwards, Beris and Grmela [26] applied a general Poisson-Bracket approach to LCP (see also the text by Beris and Edwards [27]). This approach is reduced to the Doi theory in the homogeneous (monodomain) limit. The theories [24-27] employ the same state variables as in case of low molecular mass LC, i.e. the temperature T, director $\underline{n}$ (or the respective second rank *order* tensor), and the director's space gradient $\underline{\nabla n}$. One should also mention the Rouse-like approaches to LCP developed by Volkov and Kulichikhin [28] and Long and Morse [29], which take into account the partial flexibility of LCP polymeric chains. Note that the approaches developed in papers [28, 29] did not derive the closed set of nematodynamic equations. They also cannot be considered as purely molecular, since they employed the phenomenology of paper [10] for describing the linear viscoelasticity in LCP.

Along with the above non-equilibrium molecular theories, a lot of effort was made to develop equilibrium statistical mechanics of LCP and LCE. In particular, these theories present the scalar order parameter via molecular parameters of nematics. Some recent results in this field could be found in the text [3] and papers [30, 31].

1.3. Soft Deformation Modes in LCP

Golubovich and Lubensky [32] first predicted the general possibility for occurrence of deformation *soft modes* in anisotropic elastic solids. The remarkable feature of soft modes is that they bear almost no resistance in particular direction(s) of deformed anisotropic solids. Warner and co-authors found the soft/semi-soft deformation modes for their particular molecular theory for LCE (e.g. see [3]). Yet they were unaware whether the soft modes occurred in their theory by chance or because of a more fundamental reason. An attempt to justify the occurrence of the soft modes by the rotational invariance was made in paper [33], however, not successful. The general physical idea, underlying the occurrence of soft modes in nematic solids was proposed in paper [34]. According to this paper large fluctuations typical for nematics in equilibrium, drive these systems almost to the boundary of their thermodynamic stability where the free energy is effectively minimized not only with respect to the state variables but also with respect to nematic material parameters. Thus establishing the "marginal stability" conditions could be used as a theoretical tool for finding the soft deformation modes. This approach has been first introduced in paper [35] for nematic solids and in [36] for viscous nematic LC. In real situations, there always exist small energetic barriers caused by different physical reasons which create small deformation resistance in the soft modes. These small barriers located near the boundary of thermodynamic stability, stabilize the behavior of nematic systems and constitute semi-soft (close enough to the soft) behavior of nematics. Yet, really new statistical mechanics, similar to the Goldstone theory for magnetics, should be developed to justify the occurrence of the nematic soft modes for LCE in equilibrium.

Using the marginal stability approach, the possible shearing and elongational soft/semi-soft nematic modes were recently discovered for both the weakly elastic and viscous nematics [35, 36]. In these systems, the rotational invariance of the shearing modes was found as a trivial consequence of marginal stability. Noticeable, the weak Warner elastic potential does not predict the soft elongation mode in the linear limit. The identical results of marginal stability analyses obtained for the weakly elastic and viscous nematic theories [35, 36], are explained by the fact that the well-known LEP continuum theory of nematic LC has a complete continual analog

for weakly elastic LCE proposed first by de Gennes [37]. In this analogy, the Rayleigh dissipative function in LEP theory is similar to the de Gennes monodomain elastic potential. Since the minimum of free energy functional always exists for all elastic solids, this analogy was additionally justified by demonstrating the principle of minimum of dissipation functional for viscous nematics [38]. Note that in theories describing possible soft nematic deformation modes, the number of material parameters is highly reduced.

Notably, large fluctuations are typical features for the nematic systems [34]. Therefore using attractively few-parametric mean-field molecular approaches yields poor predictions of experimental data for liquid crystals [2]. Consequently, nematic studies usually resort to continuum approaches based on fundamental principles of thermodynamics and symmetry.

As mentioned, a lot of theoretical and experimental studies have been performed to understand physics and rheological properties of lyotropic LCP's. Molecular Doi's approach with many improvements and experimental tests is well presented in the literature (e.g. see Ref. [5]). But the thermotropic LCP were poorly understood till recently, in spite of many attempts to develop either nematodynamic or molecular description of their flow properties. The beauty of continuum approach is that it can be applied to the molecular nematics of both different types, as well as to the non-yielding suspensions with shaped particles. Yet, general nematodynamic theories are multi-parametric. For example, the general LEP continuum LC theory contains five constitutive parameters [2]. Similarly, de Gennes potential proposed for the monodomain description of general weakly elastic behavior of LCE has also five parameters [37]. Because viscoelasticity is combination of elastic and viscous effects, it is expected that even in easy theoretical schemes, the continuum approach to viscoelastic polymer nematodynamics should involve at least ten constitutive parameters. This gives rise to the above pessimistic view [9] that the continuum theories of these systems are intractable.

As mentioned neither molecular nor continuum theory exist up to date for describing complicated properties of thermotropic LCP, although many experimental data for this type of LCP have been accumulated. One of objectives of the new continuum theory of weakly nonlinear viscoelastic nematodynamics [22, 23] is to interpret and simulate experimental data, and create models of processing for the LPC. New mathematical techniques [22] revealed the structure of the theory and were helpful in several derivations to present the theory in a simple form. The assumption of small transient (elastic) strains and transient relative rotations, employed in the theory, seems to be appropriate for most LCP, which usually display a small macromolecular flexibility. This assumption has been used in paper [23] to simplify the theory to symmetric type of anisotropic, fluid mechanical constitutive equations for describing the molecular elasticity effects in flows of LCP. Along with viscoelastic and nematic kinematics, the theory nontrivially combines the de Gennes general form of weakly elastic thermodynamic potential and LEP dissipative type of constitutive equations for viscous nematic liquids, while ignoring inertia effects and the Frank elasticity in liquid crystalline polymers. It should be mentioned that this theory is suitable only for monodomain molecular nematics. Nevertheless, the effects of Frank (orientation) elasticity could also be included in the viscoelastic nematodynamic theory to describe the multi-domain effects in flows of LCP's near the equilibrium. In the absence of external fields and neglecting the Frank elasticity, the simplified theory can employ less parametric description of LCP flows. Additional decrease in number of parameters happens in cases of existence of viscoelastic soft/semi-soft nematic modes [22, 23].

1.4. Specific Problems in LCP Theories

There are three additional specific problems that have to be addressed in any molecular theory for polymer nematics. The first one is a possible effect of the Frank elasticity in these systems. It was shown [3] that the Frank and molecular polymer elasticity for LCE have well separated space scales, with their crossover, the "characteristic scale" l_* evaluated as $l_* = \sqrt{K/G}$ [3]. Here $G >\sim 10^6$ dyn/cm^2 is a typical rubber-like modulus and $K \sim 10^{-7}$ dyne is a typical value of the Frank modulus. This evaluation shows that $l_* <\sim 10^{-6} cm = 10nm$, i.e. in the common macroscopic scales always larger than l_*, the effects of Frank elasticity on the nematodynamics of elastomers could be ignored.

The second problem is that the multi-domain "textures" existing at rest in many nematic LCP, affects the slow (low Deborah number) flows of LCP [5], or weak elastic deformations of LCE [3]. Although the expression for l_* could also be applied to the molecular (or "instant") elasticity of LCP, the non-equilibrium effects arising in textures do not allow ignoring the Frank elasticity effects for LCP. It looks like the mono-domain equations valid for flow of LCP in relatively strong stress/external fields, acquire near the equilibrium some stochastic or periodic properties due to the action of Frank elasticity, ignored in the mono-domain theories [38]. And *vice versa*, the polymer nematics usually forget their textures under action of higher stresses or external fields, which results in the mono-domain description. A rough method of evaluation of flow parameters based on meso-scale averaging of LEP equations over several mono-domains, involving the meso-scale averaged Frank elasticity terms has been discussed in the text [5]. Complementary to expression for characteristic space scale l_* the scaling evaluation of characteristic time of spontaneous disorientation with forming a texture of characteristic domain size δ is $t_\delta = \delta^2 \eta / K$. Here η is a characteristic viscosity for LCP near the equilibrium. Using the value $\eta \approx 10^4$ dn/cm^2 and $\delta \approx 10^{-4}$ cm for a characteristic size of domain in a typical multi-domain texture, leads to the evaluation, $t_\delta \approx 10^3$ sec, which seems to be realistic and validates the importance of the Frank elasticity in describing the slow disorientation process in some LCP's. Two time scales, one for fast stress monodomain relaxation and second for the consequent slow texture formation reported in paper [39], seem to be very common for LCP. The recent attempt to reveal the formation of texture based on a modified Doi rigid rod approach and related references can be found in paper [40].

The third problem is the possible effect of stress or external field on isotropic-nematic phase transition. In equilibrium, this phase transition is usually described by the well-known Landau phenomenology, or more specifically (however, less reliably because of large fluctuations) by the Maier-Saupe mean field theory [2] (see also recent papers [30, 31]). The assumption that the transition behavior of nematic elastomers is independent of stress was roughly confirmed in testing of the LCE theory [3], where the parameters of anisotropy were assumed to be independent of stress. The possible dependences of scalar/tensor order parameter on stress/external field have been considered in molecular Doi theory [9, 11], or phenomenological approach by Ericksen [41].

Finally, the specific nematic kinematics caused by the internal rotations as well as the macroscopic relations for moment of momentum balance in external fields have been well understood and summarized in many publications and books (e.g. see the texts [1-4] and references there). The inertial effects of internal rotations, commonly ignored in most cases for molecular nematics, might be important for nematic non-yielding suspensions and for such dynamic problems as propagation of sound in molecular nematics. In these cases, many generally small kinetic effects, such as internal spin [19] of non-nematic origin, could not be ignored too.

1.5. Experimental Effects in Flows of LCP

There are plenty of rheological experimental data, mostly obtained for liotropic LCP's, such as PBG and HPC solutions in simple shearing. They include measurements of shear viscosity and normal stress differences in steady shearing (including such features unusual for isotropic polymers as negative first normal stress difference), start up transient simple shearing, and dynamic tests with small amplitude oscillations. These data, well presented in the text [5] demonstrated exciting success of Doi theory in describing phase transition and the basic rheological properties for liotropic LCP's. It was found, however, that the above unusual rheological features predicted by Doi theory, have been observed in PBG and HPC solutions only within a range of medium concentrations: 10-25% for PBG and up to 50% for HPC. Surprisingly, the Doi rigid-rod statistical theory is incapable to describe the rheological behavior of "rigid rod" polymers [42], such as PBZT [43, 44], PBO [45] and PPTA [46]. The typical thermotropic LCP, such as thermotropic HPC and thermotropic copolyesters do not demonstrate the above unusual rheological features found in the PBG and HPC solutions and are not described by the Doi theory.

The common commercial thermotropic LCP, such as Titan (Eastman) with melting temperature $T_m = 330^0$C and Zenite 6000 (Dupont), $T_m = 345^0$C, are the random polyesters with rigid main-chain mesogenic groups. The degradation of commercial LCP's is the main problem for their rheological studies. Therefore some LCP models were synthesized, introducing either (i) flexible spacers in the main chain or (ii) mesogenic side groups. Since the melting temperature of the model LCP are far below their degradation temperatures, the model nematic LCP are convenient for rheological measurements. E.g. the LCP of (i) type have been widely used for rheological experiments [45-48].

Some specific experimental methods have also been recently elaborated and new reliable results have been obtained in rheological studies [49] of commercial thermotropic polymers, such as Titan and Zenith.

The whole sets of shearing rheological experiments for both the model and commercial thermotropic LCP's demonstrated a good consistency when pre-shearing or using preliminary orienting magnetic field, have been applied for eliminating the texture and other long memory effects. Yet it is unclear what the orientation the director acquires after pre-shearing. This uncertainty negatively affects the simulations of start up LCP flows with data obtained in standard rheometric devices. Imposing magnetic field in rheological experiments makes the initial orientation of director reliable, although it requires using non-standard rheological equipment.

LCP exhibit in simple shear steady flow several rheological effects, uncommon for polymers with long flexible chains. The first is occurring negative normal stresses observed in some LCP. The second is the effect of "three-region" viscosity shown schematically in Figure 1.

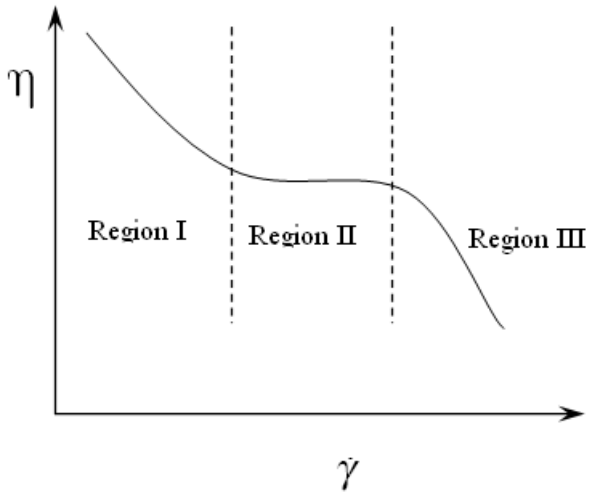

Figure 1: Schematics of three-region flow curve

This effect has been observed mostly for lyotropic LCP but sometimes was also reported for thermotropic ones. The existence of region I in this Figure 1 is explained by the formation of "texture", a domain structure observed in many, mostly lyotropic LCP. The texture occurs during relaxation when the stress levels are very low, that is when approaching the rest state. Such a three-region flow curve was first discovered in paper [50], and explained theoretically for lyotropic LCP in papers [51], [52] (see also texts [4, 5, 53]). These theoretical descriptions are typically complementary to the more fundamental monodomain nematodynamic theories of both the molecular and continuous types

Next Section employs the theory [22, 23] for simulations of steady and non-steady shearing flows. The objective is to analytically and numerically simulate these basic flows of polymer nematics with possible aligning tumbling effects, and compare the simulations with published experimental data. Hopefully, this approach will create a reliable and fundamental continuum framework for more detailed, molecular theories for polymer nematics. It is also expected that the results of present studies will significantly contribute in developing robust and reliable flow models that will be used in analyses of processing and post processing properties of polymer nematic systems. The current lack of such models prevents the progress in processing of LCP and LCE.

2. General Equations and Simulation Procedures

The simulations in this and following Sections are based on the continuum theory of weak viscoelastic nematodynamics [22, 23]. The closed set of constitutive equations includes the equation for evolution of a unit vector $\underline{n}$ called director, and anisotropic constitutive equation for evolution of extra stress tensor $\underline{\underline{\sigma}}$. In general 3D case the evolution equation for director is presented as follows:

$$\theta^*\left(\overset{00}{\underline{n}}+\underline{n}\cdot\left|\overset{0}{\underline{n}}\right|^2\right)+\overset{0}{\underline{n}}=\mathbf{b}\ \underline{n}\ \bullet\left(\lambda_e\theta^*\overset{0}{\underline{\underline{e}}}+\lambda_v\underline{\underline{e}}\right); \tag{1}$$

Here

$(\mathbf{b}(\underline{n})\bullet\underline{\underline{e}})_i=b_{ijk}(\underline{n})e_{kj}=(\delta_{ij}n_k-n_in_jn_k)e_{kj}$,

and upper circles denote the Jaumann tensor time derivatives defined as:

$$\overset{0}{\underline{n}} \equiv \dot{\underline{n}} - \underline{n}\underline{\underline{\omega}}; \qquad \overset{0}{\underline{\underline{e}}} \equiv \dot{\underline{\underline{e}}} - \underline{\underline{e}} \cdot \underline{\underline{\omega}} + \underline{\underline{\omega}} \cdot \underline{\underline{e}} \qquad \overset{0}{\underline{\underline{\sigma}}} \equiv \dot{\underline{\underline{\sigma}}} - \underline{\underline{\sigma}} \cdot \underline{\underline{\omega}} + \underline{\underline{\omega}} \cdot \underline{\underline{\sigma}} \ .$$

Equation **(1)** is coupled with anisotropic equation for evolution of extra stress tensor $\underline{\underline{\sigma}}$:

$$\begin{aligned} \theta_0 \overset{0}{\underline{\underline{\sigma}}} + \underline{\underline{\sigma}} + (r_1 - 1)\left[\underline{nn} \cdot \underline{\underline{\sigma}} + \underline{\underline{\sigma}} \cdot \underline{nn} - 2\underline{nn}(\underline{\underline{\sigma}} : \underline{nn})\right] + 1.5(r_2 - 1)(\underline{nn} - \underline{\underline{\delta}}/3)(\underline{\underline{\sigma}} : \underline{nn}) \\ = \eta_0 \left[\underline{\underline{e}} + \alpha\left[\underline{nn} \cdot \underline{\underline{e}} + \underline{\underline{e}} \cdot \underline{nn} - 2\underline{nn}(\underline{\underline{e}} : \underline{nn})\right] + (\beta - 3/2)(\underline{nn} - \underline{\underline{\delta}}/3)(\underline{\underline{e}} : \underline{nn})\right] . \end{aligned} \tag{2}$$

In equations **(1)–(2)**, G_0 and η_0 are characteristic nematic modulus and viscosity, $\theta_0 = \eta_0 / G_0$ and θ^* $(\sim\theta_0)$ are the relaxation times, λ_e and λ_v are the elastic and viscous tumbling parameters, α, β and r_1, r_2 are parameters characterizing anisotropy, $\underline{nn}$ is dyadic with components $n_i n_j$, $\underline{\underline{e}}$ and $\underline{\underline{\omega}}$ are the strain rate and vorticity tensors commonly related to the gradient velocity tensor. The constitutive equations **(1), (2)** should be consistently used along with the momentum balance equation to determine both the stress and flow fields. In few cases, however, the flow field is known. One of these flows, having many practical applications, is simple shearing. In this flow, solution of constitutive equations for weakly nonlinear viscoelastic nematodynamic can be simplified.

The shearing flows are commonly analyzed using a "standard" Cartesian coordinate system $\{x_1, x_2, x_3\}$ where x_1 is directed along the flow and x_2 along the velocity gradient. In this coordinate system, the velocity vector $\underline{v}$ is: $\underline{v} = \{\dot{\gamma}(t) x_2, 0, 0\}$, and the tensors of strain rate $\underline{\underline{e}}$ and vorticity $\underline{\underline{\omega}}$ for homogeneous shearing flows have the matrix forms:

$$\underline{\underline{e}}\ t = \frac{\dot{\gamma}\ t}{2}\begin{pmatrix} 0 & 1 & 0 \\ 1 & 0 & 0 \\ 0 & 0 & 0 \end{pmatrix}, \qquad \underline{\underline{\omega}}\ t = \frac{\dot{\gamma}\ t}{2}\begin{pmatrix} 0 & -1 & 0 \\ 1 & 0 & 0 \\ 0 & 0 & 0 \end{pmatrix} \tag{3}$$

Here the shear rate $\dot{\gamma}(t)$ is a given function of time. We will use below a common simplifying assumption that vector of director is located in shear plane, so the 2D expression for director is $\underline{n} = \{n_1, n_2, 0\}$. Substituting this expression along with **(3)** into evolution equation **(1)** yields the evolution equation for the longitudinal component n_1 of director located in the $\{x_1, x_2\}$ shear plane as:

$$\theta^*\left(\ddot{n}_1 + \frac{n_1 \dot{n}_1^{\,2}}{n_2^{\,2}}\right) + \dot{n}_1 - \frac{\dot{\gamma} n_2}{2} = \theta^* \ddot{\gamma}[\lambda_e(1 - 2n_1^{\,2}) + 1]\frac{n_2}{2}/2 + \lambda_e \theta^* \dot{\gamma}^2 n_1 n_2^{\,2} + \frac{\lambda_v \dot{\gamma} n_2}{2}(1 - 2n_1^{\,2}), \tag{4}$$

Here $n_2 = \sqrt{1 - n_1^{\,2}}$.

In simple shearing flow, equation **(2)** is rewritten in component form as:

$$\begin{aligned} &\theta_0 \frac{d\sigma_{12}}{dt} + \theta_0 \dot{\gamma} \frac{\sigma_{11} - \sigma_{22}}{2} + \sigma_{12} + (r_1 - 1)\left[\sigma_{12} + n_1 n_2 (\sigma_{11} + \sigma_{22})\right] + \sigma_{11} n_1^{\,2} + \sigma_{22} n_2^{\,2} + 2\sigma_{12} n_1 n_2 \\ &n_1 n_2\left[\frac{3}{2}(r_2 - 1) - 2(r_1 - 1)\right] = \frac{\eta_0 \dot{\gamma}}{2}\left(1 + \alpha + 2n_1^{\,2} n_2^{\,2}\left(\beta - 2\alpha - \frac{3}{2}\right)\right) \end{aligned} , \tag{5a}$$

$$\theta_0 \frac{d\sigma_{11}}{dt} - \sigma_{12}\theta_0\dot{\gamma} + \sigma_{11} + 2\ r_1 - 1\quad \sigma_{11}n_1^{\ 2} + \sigma_{12}n_1n_2\ + \left[\frac{3}{2}\ r_2 - 1\left(n_1^{\ 2} - \frac{1}{3}\right) - 2\ r_1 - 1\ n_1^{\ 2}\right],$$
$$\times\ \sigma_{11}n_1^{\ 2} + \sigma_{22}n_2^{\ 2} + 2\sigma_{12}n_1n_2\ = \eta_0\dot{\gamma}n_1n_2\left(\alpha\ 1 - 2n_1^{\ 2}\ + \left(\beta - \frac{3}{2}\right)\times\left(n_1^{\ 2} - \frac{1}{3}\right)\right) \quad (5b)$$

$$\theta_0 \frac{d\sigma_{22}}{dt} + \sigma_{12}\theta_0\dot{\gamma} + \sigma_{22} + 2\ r_1 - 1\quad \sigma_{22}n_2^{\ 2} + \sigma_{12}n_1n_2\ + \left[\frac{3}{2}\ r_2 - 1\left(n_2^{\ 2} - \frac{1}{3}\right) - 2\ r_1 - 1\ n_2^{\ 2}\right].$$
$$\times\ \sigma_{11}n_1^{\ 2} + \sigma_{22}n_2^{\ 2} + 2\sigma_{12}n_1n_2\ = \eta_0\dot{\gamma}n_1n_2\left(\alpha\ 1 - 2n_2^{\ 2}\ + \left(\beta - \frac{3}{2}\right)\left(n_2^{\ 2} - \frac{1}{3}\right)\right) \quad (5c)$$

Equations **(5a-c)** describe the time dependent evolution and steady behavior of extra stress tensor in simple shearing.

In case of steady shearing analyzed in paper [23], the analytical expression for horizontal component of director n_1 was found as:

$$n_1^2 = \frac{1}{2}\left(1 + \lambda_{\text{v}}\frac{1 + \left|D\lambda_1/\lambda_{\text{v}}\right|\sqrt{D^2\lambda_e^2 + \lambda_{\text{v}}^2 - 1}}{D^2\lambda_e^2 + \lambda_{\text{v}}^2}\right)., \quad (6)$$

here $D = \theta * \dot{\gamma}$. In this case a very awkward analytical solution of equations **(4), (5a-c)** has also been obtained using "*Mathematica*" software. Formula (6) shows that the director position weakly depends on elastic tumbling parameter λ_e and strongly depends on the value of viscous tumbling parameter λ_{v}. The same aligning condition $\left|\lambda_{\text{v}}\right| > 1$ as in viscous case holds in viscoelastic nematodynamics. As compared to the Ericksen theory, the new fact here is the dependence position of director $\underline{n}$ on the flow Deborah number De. This dependence delays the onset of the rest state tumbling and tends to orient the director along or perpendicular flow lines when $\lambda_{\text{v}} > 0$ or when $\lambda_{\text{v}} < 0$, respectively. The dependence $\underline{n}$ on De mostly contributes to the shear thinning effect where the sign of the first normal stress difference N_1 depends on the sign of λ_{v}, with $\left|N_1\right|$ growing with increasing $\dot{\gamma}$.

In case of relaxation, the expression for horizontal component of director $n_1(t)$ was explicitly obtained in [23] as the solution of **(4)** using presentation $n_1(t) = \cos\varphi(t)$:

$$\varphi(t) = \varphi_0 + D\lambda_e(1 - e^{-t/\theta^*})\cos 2\varphi_0, \quad (7)$$

here the value $\varphi_0(D)$ is known from **(6)**. In case of relaxation the values of stress components are found in this Chapter by numerical solution of set of ODE **(5a-c)**, with the use of formula **(7)**.

In case of start up flow from the rest state, a numerical solution of ODE set **(4)** - **(5a-c)** should be obtained using the following initial conditions:

$$\underline{\underline{\sigma}}\big|_{t=0} = 0; \qquad n_1\big|_{t=0} = n_{1r}; \quad \dot{n}_1\big|_{t=0} = n_{2r}\dot{\gamma}_0[\lambda_e(1 - 2n_{1r}^{\ 2}) + 1]/2. \quad (8)$$

The first condition in (8) is the natural (zero) initial conditions for the stress tensor in start up shearing flow

from the rest state. To resolve the problem of choosing the initial condition n_{1r} for director in start up flow we preliminarily fitted the experimental data for stresses in steady shearing with following adjustment of parameters to describe also the stress relaxation. In this case the parameters of evolution equation for director, along with its orientation in steady shearing were also established. Calculating then the orientation of director during stress relaxation we found its final orientation at the rest state, which was taken as initial director value $\underline{n}_r$ in the start up flow. Thus the value of parameter n_{1r} is established as the fully relaxed value of director after relaxation. Using formula (7) in the limit $t \to \infty$, the value of n_{1r} is found as:

$$n_{1r} = \cos\varphi_r; \qquad \varphi_r = \varphi_0 + D[\lambda_e \ (1 - n_{1,0}^2) \quad 1. \tag{9}$$

The second initial condition in (**8**) is derived from equation **(4)** using initial jump (or delta) conditions.

In the following we compare the results of numerical simulations with published shearing experimental data, generally presented as time dependent plots for shear stress σ_{12}, apparent viscosity $\eta = \sigma_{12}/\dot{\gamma}$, and the "first normal stress difference" $N_1 = \sigma_{11} - \sigma_{22}$. The shearing flow simulations include the steady shearing, relaxation, and transient start-up flows. To analyze simple shearing flows for aligning thermotropic LCP's, we will use in the following the monodomain CE's (4), (5a-c) with above formulas (6) – (9) suitable for specific problems.

The ultimate goal of simulations was to show a very possibility to describe experimental data along with determining the constitutive parameters. These parameters established for steady shearing are then used for calculating evolution of director, shear stress and first normal stress difference during relaxation and start up flow.

To resolve the problem of choosing the initial conditions for director in start up flow we preliminarily fitted the experimental data for stresses in steady shearing with following adjustment of parameters to describe also the stress relaxation. In this case the parameters of evolution equation for director, along with its orientation in steady shearing were also established. Calculating then the orientation of director during stress relaxation we found its final orientation at the rest state, which was taken as initial director value in the start up flow.

3. LCP and their Parameters Established in Simulations

Common commercial thermotropic LCP's are the random polyesters with rigid main-chain mesogenic groups. These LCP's have very narrow time and temperature intervals between beginning the crystal melting and onset of polymer degradation, where the liquid crystalline phase exists. The existence of multi-domains in these commercial thermotropic LCP's has not been reported, and it seems improbable because of short time processing. The degradation of commercial LCP's is the main problem for their rheological studies. Therefore some "model" LCP's have been synthesized in various laboratories. The main objective of the model LCP was to incorporate flexible spacers or pendent bulky group into the main chain and then reduce the melting point T_m and the clearing temperature T_{cl} of LCP's, which are far below their degradation temperature T_d. Using these techniques it was possible to safely run the rheological measurements within the temperature intervals

below T_d.

Our simulations of the above viscoelastic nematodynamics theory require the reliable and representative rheological data for LCP, obtained for steady and transient shear flows, and relaxation. We chose literature rheological data for two commercial LCP's, Titan and Zenith 6000 [49], as well as for two model polymers, a main-chain LCP - PSHQ9 and a side-chain LCP - PI-14-5CN [53].

According to [49] two commercial random copolyesters, Titan and Zenith 6000 were obtained from the Eastman and DuPont Chemical companies, respectively. These LCP have very narrow time and temperature intervals between beginning the crystal melting and onset of polymer degradation, where the liquid crystalline phase exists. The existence of multi-domains in these commercial thermotropic LCP's has not been reported, and because of short time processing, it seems to be improbable.

Titan is random copolyester probably composed of two random units, ethylene-terephthalate (PET) and hydroxybenzoic acid (HNA). Incorporating the PET unit in the main chain reduces the rigidity of the molecule due to the two methylene flexible spacers, and in turn decreases the melting temperature of the material. On the other hand, Zenith 6000 is fully aromatic, where kinks were introduced by combining phenol and biphenol molecules by random copolymerization. As measured by DSC, the melting temperature T_m of Titan was between 325 and 335 ^{0}C, while for Zenith 6000, T_m was between 340 and 360 ^{0}C. TGA measurements indicated that the degradation temperature T_d of Titan is 450 ^{0}C, although it has been reported in [49] that the noticeable degradation begins at considerably lower temperatures.

One typical example of model LCP is PSHQ9 - poly[(phenylsulfonyl)-*p*-phenylene nonanemethylene bis(4-oxybenzoate)] [54] whose chemical structure depicted in Figure 2. This is a main-chain LCP, which has a glass transition temperature T_g of 84 °C, and a nematic-to-isotropic (N-I) transition temperature T_{NI} of 162 °C. This polymer has only nematic phase at temperatures between T_g and T_{NI}.

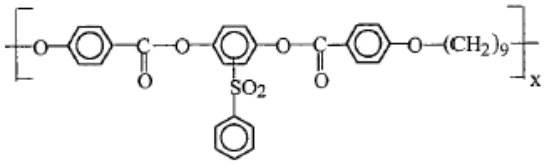

PSHQ9

Figure 2: Chemical structure of PSHQ9 [54]

Another typical model LCP is PI-14-5CN. It is a nematic side-chain liquid-crystalline polymer (SCLCP), with the chemical structure [54] presented in Figure 3. A nearly monodisperse PI-14-5CN was synthesized using anionic polymerization by grafting a liquid-crystalline monomer, 6-[(4-cyano-4□-biphenyl)oxy]hexanoic acid (5CN-COOH), onto a nearly monodisperse hydroxylated polyisoprene (PI). This polymer undergoes glass transition at 45 °C and N-I transition at 102 °C.

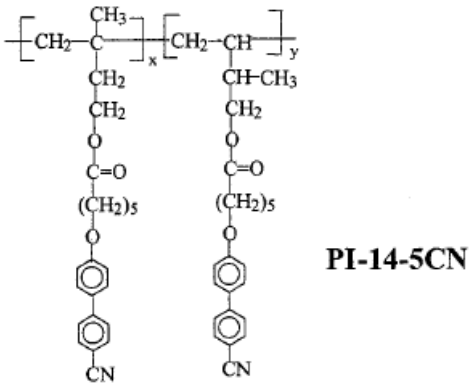

Figure 3: Chemical structure of PI-14-5CN [54]

It is significant that almost all the model SC LCP's reported in the literature have been synthesized by condensation polymerization, invariably giving rise to polydisperse SC LCP's. It was impossible to precisely determine the molecular weight of PI-14-5CN from the GPC because of lack of information on its hydrodynamic volume. So the molecular weight was approximately calculated to be 7.19×10^4 g/mol using information on the degree of hydroxylation. The polydispersity of PI-14-5CN found from GPC was equal to 1.08.

The values of constitutive parameters for all tested LCP's, obtained by the mentioned intense fitting procedure are shown in Tables 1 and 2.

Table 1: Parameters of anisotropy and tumbling for industrial and model LCP's

LCP	α	β	r_1	r_2	λ_e	λ_v
Titan $340\,^0C$	0.2	0.5	0.15	0.222	2.2	30
Zenith 6000 $360\,^0C$	4	0.1	0.55	0.367	1.01	50
PSHQ9 $70,80,90\,^0C$	0.7	1.3	0.5	0.9	2	12
PI-14-5CN $130,140,150\,^0C$	5	8	0.7	0.533	2	18

Table 2: Viscoelastic parameters for industrial and model LCP's

LCP	**Titan** $340\,^0C$	**Zenith 6000** $360\,^0C$	**PSHQ9** temperatures ^0C:			**PI-14-5CN** temperatures ^0C:		
			70	80	90	130	140	150
Relaxation time θ_0, sec	0.3	2.5	1.5	0.8	0.28	3	2.8	2.2
Viscosity η_0, kPa·sec	0.34	1.55	200	9	2.9	220	70	10

When comparing the values of constitutive parameters found for Titan and Zenith 600, one should recall that Titan is random copolyester of ethylene-terephthalate (PET) and hydroxybenzoic acid (HNA) with two

methylene flexible spacers, whereas Zenith 6000 is a fully aromatic copolyester with kinks. Therefore Zenith 6000 is expected to be much more rigid than Titan. Our simulations confirmed this. They demonstrate that the values of viscoelastic parameters θ_0 and η_0, parameter of viscous tumbling λ_v, and anisotropy parameters α, r_1 and r_2 found for Titan are smaller than those of Zenith 6000, while the values of elastic tumbling parameter λ_e and the anisotropic parameter β for Titan are greater than those for Zenith 6000.

It is also seen that all the constitutive parameters for PSHQ9, except r_2 and λ_e, are larger than those for PI-14-5CN. We remind that PSHQ9 is a main-chain LCP, whereas PI-14-5CN is a side-chain one. The flexible main chain in PI-14-5CN makes it much easier to relax and decouple the mesogens from the main chain. In contrast, the main-chain LCP (PSHQ9) possesses mesogens in the main chain, which are tightly packed together and in turn have relatively low mobility and capability of relaxation.

4. Results of Simulations

4.1 Simulations of Steady Shearing Flows

Figure 4 demonstrates the experimental data and fitting curves for effective viscosity □, shear stress □$_{1}$□, and first normal stress difference N_1 versus shear rates $\dot{\gamma}$ for Titan at 340 ^{o}C.

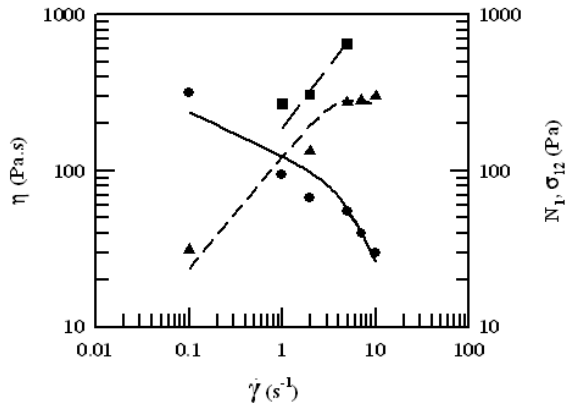

Figure 4: Experimental data for apparent viscosity □ (●), shear stress □$_{1}$□ ▲), and the first normal stress difference N_1 (■) versus shear rate $\dot{\gamma}$ for Titan at 340 ^{o}C. Fitting curves are shown by solid line for □, short dash line for □$_{1}$□, and by long dash line for N_1.

Here the constitutive parameters were found by the curve fitting procedure. As seen, there is a good agreement between simulations and experimental data. However, the fitting curve for apparent viscosity □ does not exhibit the general three region flow curve [8]. It is probably because only a narrow part of region II has been presented in the experimental data. The region I should appear at very low shear rates $\dot{\gamma}$ if there is a texture, which the current monodomain approach is incapable to describe. It should also be noted that the first normal stress difference is positive in the range of shear rates investigated.

Figure 5 demonstrates the flow curve for Zenith 6000 at 360 ^{o}C, presented as the logarithmic plot of apparent shear viscosity □ versus shear rate $\dot{\gamma}$.

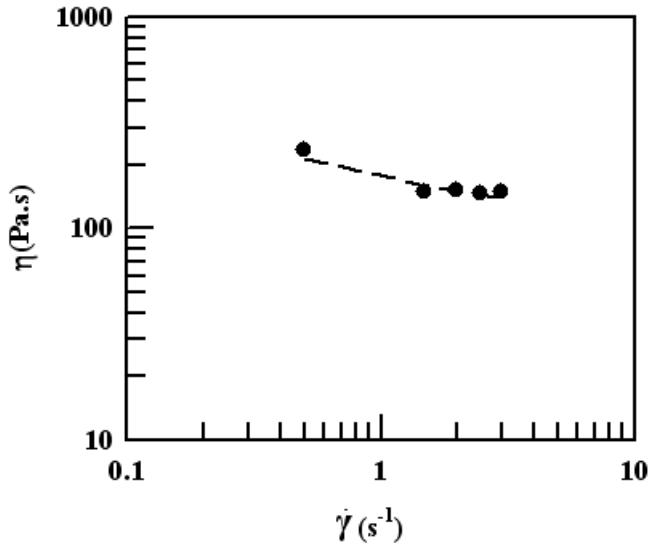

Figure 5: Experimental data (dots) and fitting curve (dashed line) for the logarithmic plot of viscosity □ versus shear rate $\dot{\gamma}$ for Zenith 6000 at 360 °C.

In Figure 5, the experimental results are shown by dots and the fitting curve by dashed line. Unfortunately, the normal stress data for this polymer were not reported. It is unclear whether the experimental plot is related to the transition from the region I to region II in the general three-region viscosity plot.

Figure 6 shows steady shearing experimental data for PSHQ9 at different temperatures in the nematic region. Presented here are the logarithmic plots for apparent viscosity η and the first normal stress difference N_1 versus shear rate $\dot{\gamma}$. The viscosities of both experimental data and fitting curves exhibit regions II and III, and the Newtonian behavior becomes obvious as the temperature increases.

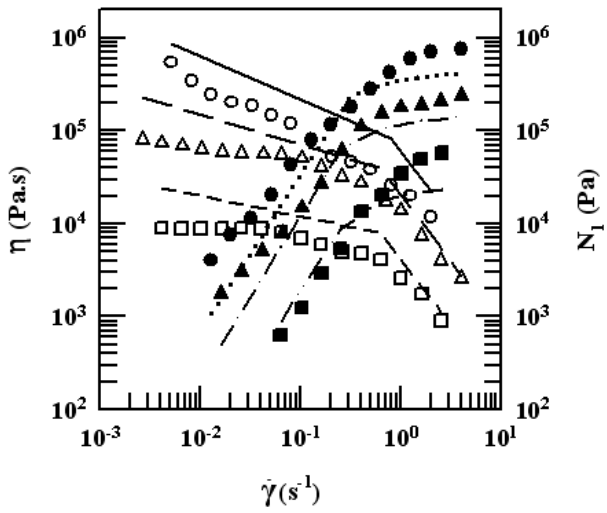

Figure 6: Experimental data for dependences of apparent viscosity η (open symbols) and first normal stress difference N_1 (filled symbols) on shear rate $\dot{\gamma}$ for PSHQ9 in steady flow at different temperatures in the nematic region:(○,●) 130 °C; (Δ, ▲) 140°C; (□, ■) 150°C. The fitting curves for plots of log η versus log $\dot{\gamma}$ are shown as: at 130 °C (solid line), 140°C (long dashed line), and 150°C (short dash line). The fitting curves for log N_1 versus log $\dot{\gamma}$ use the same curve symbols.

Both experimental and simulated data for N_1 are positive over the range of shear rates investigated. The viscosity of PSHQ9 exhibits a shear-thinning at very low values of $\dot{\gamma}$, a Newtonian behavior at its intermediate values, and then, again, a strong shear-thinning behavior at higher values of $\dot{\gamma}$. However, as the temperature increases from 130 to 140 ^{0}C, the region I in the η plot for PSHQ9 becomes very weak, and when the temperature increases further to 150^{o}C, the region I disappears. Since PSHQ9 is a polydisperse polymer, the low molecular fraction of PSHQ9 can transform into the isotropic state, forming a biphasic state before reaching T_{NI} (ca. 160^{o}C). Thus, the nematic property of PSHQ9 becomes progressively weaker as the temperature approaches T_{NI}. In such situations, region I in the η plot for PSHQ9 may not be observable.

Figure 7 shows the logarithmic plots of steady shearing experimental data (dots) for η and N_1 versus $\dot{\gamma}$ for PI-14-5CN at different temperatures. Corresponding fitting curves are shown by lines. It is seen that the fitting curves for both η and N_1 are in an excellent agreement with experimental data, being better than those for PSHQ9. The viscosity of PI-14-5CN exhibits a Newtonian behavior at low $\dot{\gamma}$ values and then shear-thinning behavior, while the first normal stress difference N_1 is positive over the entire range of $\dot{\gamma}$ tested at three temperatures in the nematic region. The absence of region I in the η plots might be due to the fact that PI-14-5CN is a side-chain LCP, and its nematic behavior is not sufficiently strong. The above observation supports the view [7] that region I in the η plots for various LCP's is associated with the existence of domain structure.

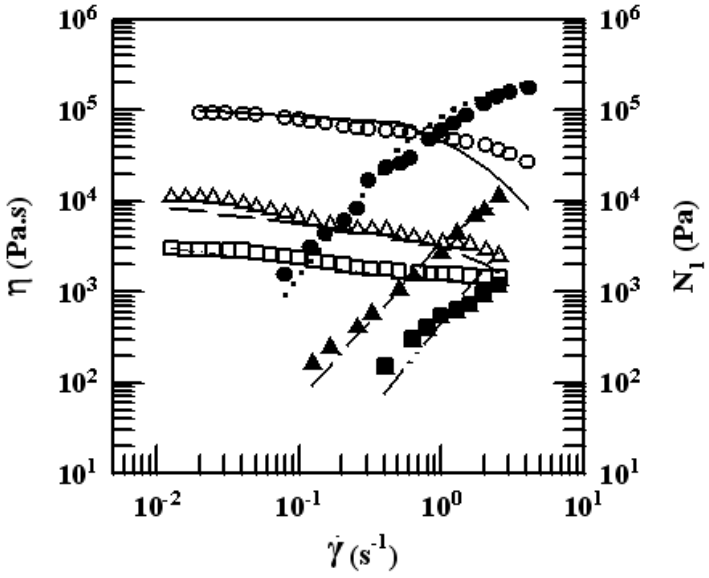

Figure 7**:** Experimental data for dependences of apparent viscosity η (open symbols) and first normal stress difference N_1 (filled symbols) on shear rate $\dot{\gamma}$ for PI-14-5CN in steady flow at different temperatures in the nematic:(○,●) 70 °C; (Δ, ▲) 80°C; (□, ■) 90°C. The fitting curves for plots of $\log\eta$ versus $\log\dot{\gamma}$ are shown as: 70 °C (solid line), 80°C (long dash line), and 90°C (short dash line). The same curve symbols are used for fitting plots of log N_1 versus $\log\dot{\gamma}$ at different temperatures.

4.2 Simulations of Transient Start-up Shear Flows

In the following we will use normalized stresses denoting by additional + symbol the time dependent shear and normal stresses. The absence of + symbols indicates the stresses in steady flow.

The appearance of multiple overshoots in the first normal stress difference in transient shear flow can be qualitatively explained using molecular theory by Marrucci-Maffettone [9]. This monodomain theory is based on the Maier-Saupe potential, which is valid for low-molecular weight thermotropic liquid crystals. Therefore it may not be suitable for semi-flexible main-chain LCP exhibiting flow aligning behavior. On the other hand, the Larson-Doi mesoscopic model [10] describes the evolution of texture based on some experimental observations of decrease in domain size with increasing shear rate and growing domain size upon cessation of flow. Although the Larson-Doi mesoscopic model [10] for LCP's qualitatively predicts the experimental observations for the time evolution of shear □ $\dot{\gamma}$,t) and normal □₁$\dot{\gamma}$,t)stresses in start up flows, the predicted magnitude of □ $\dot{\gamma}$,t) is lower than that of □₁$\dot{\gamma}$,t)/□₁. This contradicts to experimental observations [20]. Furthermore, the models [9, 10] predict a much shorter transient time (strain) for □ $\dot{\gamma}$,t)and □₁$\dot{\gamma}$,t)variations as compared with experimental data. The inadequacy of the Larson-Doi model to accurately predict the time evolution of □₁$\dot{\gamma}$,t) in transient shear flow can be explained by the presence of long flexible spacers and bulky pendent side groups in the LCP's. Both the long flexible spacers and bulky pendent side groups in LCP macromolecules might directly suppress molecular rotations and perhaps, collective molecular rotations, or director tumbling. Although the Larson-Doi mesoscopic model is currently the only one existing model that describes polydomain texture and distortional elastic effects, the model is based on the Leslie-Ericksen equations, which is appropriate either for low molecular liquid crystals or lyotropic systems that have short relaxation times.

It seems that the majority of thermotropic LCP's exhibit flow aligning behavior. Thus to describe the experimental observations for these polymers, the general viscoelastic nematodynamics theory [16, 17] is used in our simulations with aligning assumption.

Figures 8 and 9 demonstrate the start-up shear flow at $\dot{\gamma} = 6\,s^{-1}$ for Titan at 340 °C. Figure 8 shows the evolution of normalized shear stress □ $\dot{\gamma}$,t)/□̇ with strain ($\dot{\gamma}$t) and Figure 9 the normalized first normal stress difference □₁$\dot{\gamma}$,t)/□₁. Here the experimental data are denoted by dots and simulated curves by dashed line. As seen both the shear stress and the first normal stress difference display large and broad overshoots at $\dot{\gamma}t \approx 50$. Since Titan has very rigid macromolecules, the evolution of texture is slow, and in turn the overshoot occurs at high value $\dot{\gamma}$t .

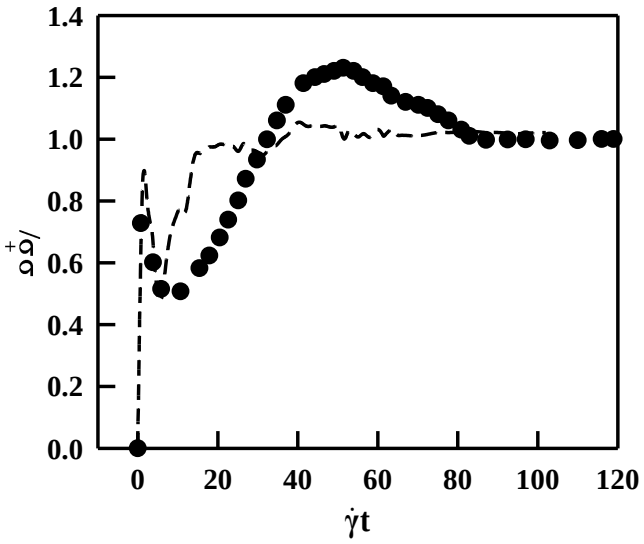

Figure 8: The evolution of normalized shear stress □ $\dot{\gamma}$,t)/σ with strain ($\dot{\gamma}$t) for Titan at 340 °C in start-up shear flow at $\dot{\gamma} = 6\,s^{-1}$: experimental data are shown by dots, and simulated curve by dashed line.

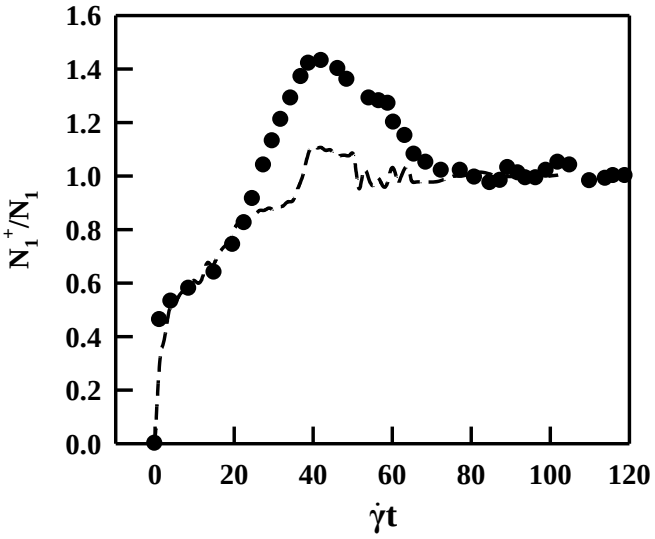

Figure 9: The evolution of normalized first normal stress difference □₁$\dot{\gamma}$,t)/□₁with strain ($\dot{\gamma}$t) for Titan at 340 °C in start-up shear flow at $\dot{\gamma} = 6\,s^{-1}$; notations are same as in Figure 8.

Figure 10 demonstrates the evolution of shear stress □with strain ($\dot{\gamma}$t) for Zenith 6000 at 360 °C in start-up shear flow at $\dot{\gamma} = 2\,s^{-1}$. The experimental data are shown by dots and simulated curve by dashed line. The data for shear stress initially exhibit a small overshoot at $\dot{\gamma}t \approx 4$ and a large and broad overshoot at $\dot{\gamma}t \approx 76$. In the simulated curve, a small overshoot occurs at $\dot{\gamma}t \approx 16$ and a large overshoot at $\dot{\gamma}t \approx 50$.

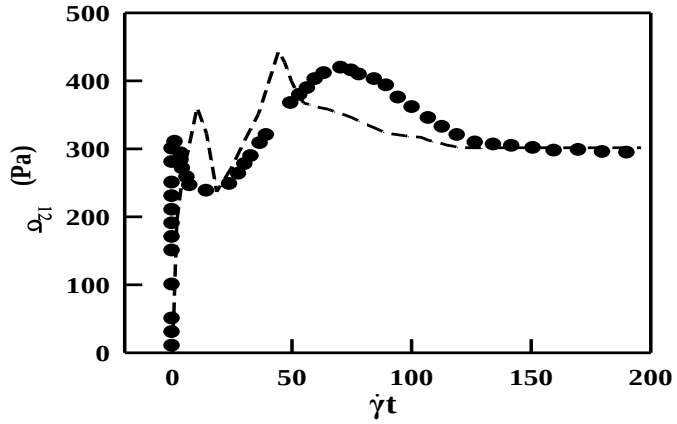

Figure 10: The evolution of shear stress □with on strain ($\dot{\gamma}$t) for Zenite 6000 at 360°C in start-up shear flow at $\dot{\gamma} = 2\,s^{-1}$: notations are the same as in Figure 8.

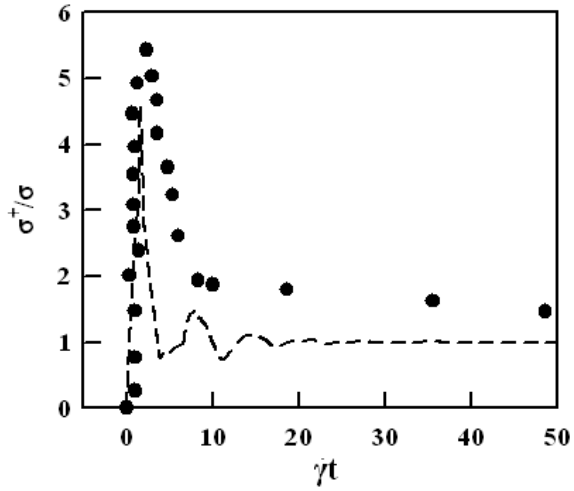

Figure 11: The evolution of normalized shear stress □ γ̇,t)/□with strain (γ̇t) for PSHQ9 at 130 °C in start-up shear flow at $\dot{\gamma} = 1 s^{-1}$: notations are the same as in Figure 8.

Figures 11 and 12 describe the evolution of normalized shear stress □ γ̇,t)/□and first normal stress difference N_1 γ̇,t)/$N_1$with strain γ̇t for PSHQ9 in start-up shear flow. The flow temperature was 130 °C and shear rate is $\dot{\gamma} = 1 s^{-1}$. The experimental data are shown by dots and simulated curves by dashed line. The simulated overshoots for shear and normal stresses are the same as those for experimental data, but the overshoots in calculated curves occur at a relatively low γ̇t and are very narrow. One can attribute such large values of □ γ̇,t)/□ ratios, characteristic for liquid crystalline polymers, to the existence of a lot of polydomains in the nematic state when the start-up flow initiated. Recall that the theory used
for simulation utilizes monodomain approach, whereas PSHQ9 exhibits polydomains in nematic state in start-up flow. Thus deviation of simulated results from experimental data seems reasonable.

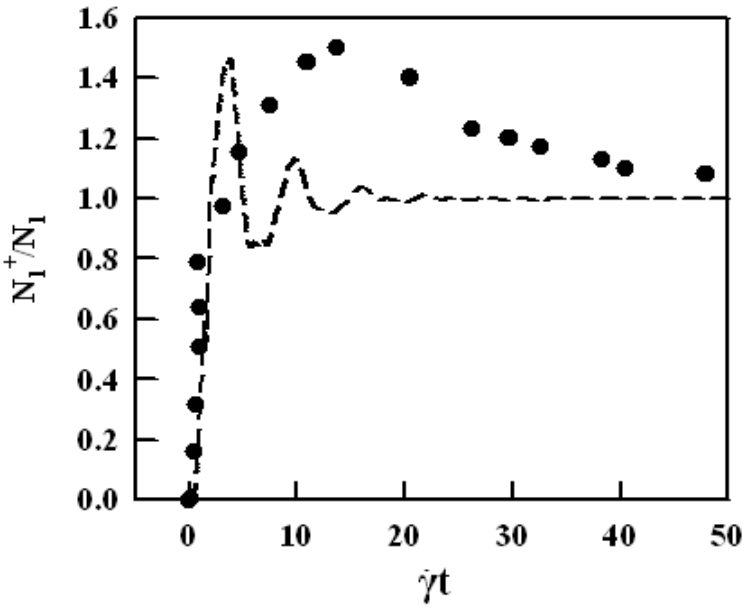

Figure12: The evolution of normalized first normal stress difference N_1 γ̇,t)/$N_1$with strain (γ̇t) for PSHQ9 at 130 °C in start-up shear flow at $\dot{\gamma} = 1 s^{-1}$: notations are the same as in Figure 8.

Figures 13 and 14 describe, respectively, the evolution of normalized shear stress □ $\dot{\gamma}$,t)/□and first normal stress difference $N_1\dot{\gamma}$,t)/$N_1$with strain $\dot{\gamma}$t for PI-14-5CN at 70 °C in start-up shear flow at $\dot{\gamma}=1s^{-1}$. In these figures, experimental data are shown by dots and fitting curve by dashed line. The experimental data for both the shear and normal stresses exhibit large overshoots and then decay to steady values. The simulated evolution of normalized shear stress with strain is fitted well enough with experimental data, whereas there is a relatively large difference between the simulated curve for normal stress and experimental data. This once again may be attributed to simulating the polydomain LCP using monodomain theory.

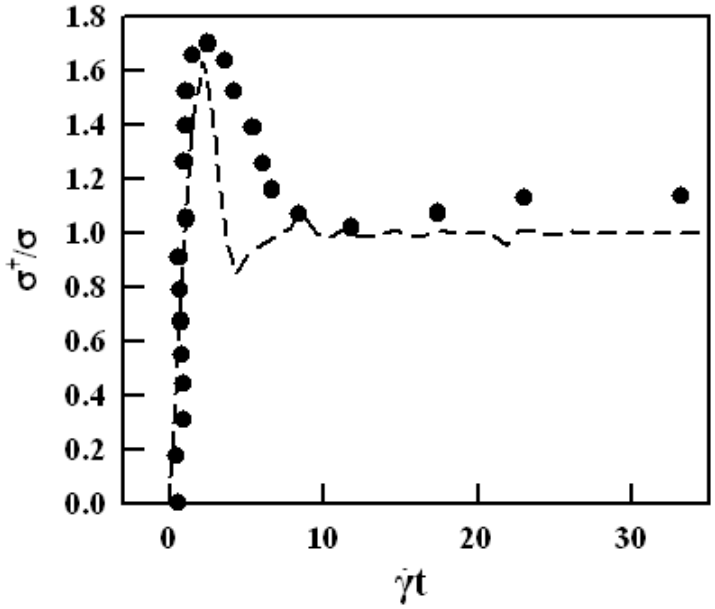

Figure 13: The evolution of normalized shear stress □ $\dot{\gamma}$,t)/□ with strain ($\dot{\gamma}$t) for PI-14-5CN at 70 °C in start-up shear flow at $\dot{\gamma}=1s^{-1}$: notations are the same as in Figure 8.

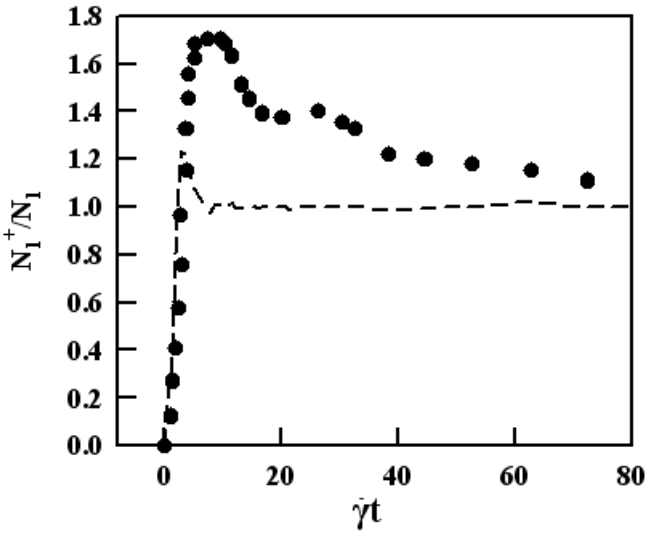

Figure14: The evolution of normalized first normal stress difference $N_1\dot{\gamma}$,t)/$N_1$with strain ($\dot{\gamma}$t) for PI-14-5CN at 70 °C in start-up shear flow at $\dot{\gamma}=1s^{-1}$: notations are the same as in Figure 8.

As compared to Figures 11 and 12, in start-up shear flow the overshoot peak for normal stress occurs much sooner in PI-14-5CN than in PSHQ9, while the overshoot peak in shear stress occurs very quickly in both PI-14-5CN and PSHQ9. The overshoot peak value of fitted normal stress for PSHQ9 is slightly larger than that of PI-14-5CN, while the overshoot peak value of shear stress for PSHQ9 is about 3-4 times greater than that of PI-14-5CN. Thus, the transient responses in first normal stress difference and shear stress for side-chain LCP, PI-14-5CN are quite different from those for main-chain LCP, PSHQ9. In the latter case, 5CN-COOH mesogens are grafted onto the coil-like PI forming a polymer backbone through five methylene groups as flexible spacer. So the motions of the polymer backbone and the 5CN-COOH mesogens in PI-14-5CN may be regarded as being partially decoupled, making the 5CN-COOH mesogens mobile during shear flow [20]. Further, each mesogen grafted onto the backbone of PI-14-5CN may move or orient, upon start-up of shear flow, slightly depending on other mesogens. On the other hand, the mesogens in PSHQ9 are directly linked to the polymer backbone, making motions of the mesogens and backbone of PSHQ9 strongly coupled during shear flow. Thus, each mesogen in PSHQ9 cannot act as independent, i.e. all the mesogens in PSHQ9 act in start-up of shear flow collectively or cooperatively.

4.3 Simulations of Relaxation after Cessation of Steady Flow

Figures 15 and 16 show the relaxation of shear stress σ_{12} and first normal stress difference N_1 respectfully, for Titan at 340°C after cessation of steady flow with shear rate $\dot{\gamma} = 6\,s^{-1}$. Here experimental data are shown by dots and fitting curve by dashed lines. The values of both σ_{12} and N_1 during relaxation drop abruptly and reach zero at the time of around 4 s. The simulated relaxation curve for σ_{12} has an excellent agreement with the experimental data, but this is not the case for N_1 when t > 4 s. This disagreement is seemingly attributed to the experimental error, because the final value of N_1 during relaxation should reach zero.

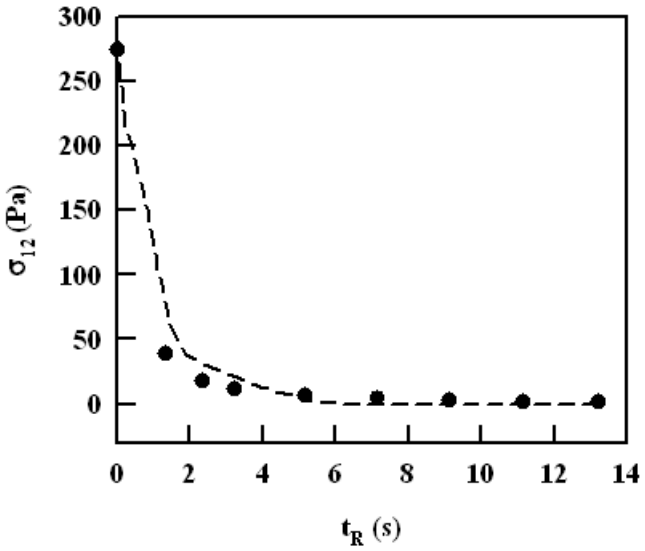

Figure 15: Relaxation of shear stress σ_{12} for Titan at 340 °C upon cessation of steady flow at shear rate $\dot{\gamma} = 6\,s^{-1}$: experimental data are shown by dots and simulated curve by dashed line.

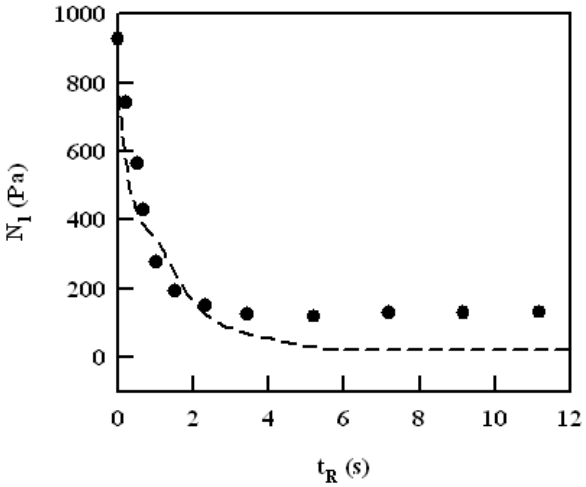

Figure16: Relaxation of first normal stress difference N_1 for Titan at 340 °C upon cessation of steady flow at shear rate $\dot{\gamma} = 6\,\mathrm{s}^{-1}$: notations are the same as in Figure 15.

Figure 17 presents the relaxation of normalized (a) shear stress and (b) the first normal stress difference upon cessation of steady shear flow at $\dot{\gamma}$ = 0.5 s^{-1} for PSHQ9 at 130°C. Here experimental data are shown by dots and fitting curve by dashed line. The normalizing values σ_0 and $N_{1,0}$ are the steady values of shear stress and the first normal stress difference, respectively, just prior to flow cessation. As seen the normalized shear stress approaches to zero at t_R > 7 s, whereas the normal stress reaches zero when t_R > 15 s.

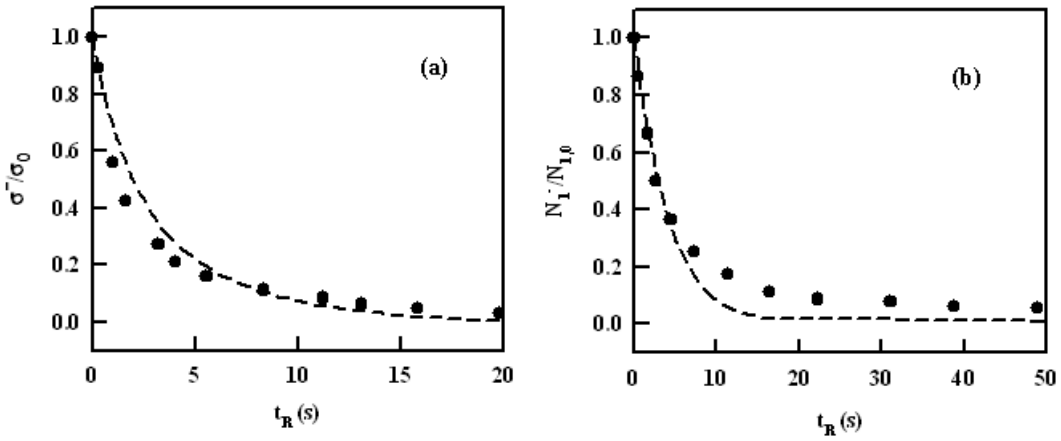

Figure 17: Relaxation of normalized (a) shear stress, $\sigma^-(t)/\sigma_0$ and (b) first normal stress difference, $N_1^-(t)/N_{1,0}$ upon cessation of steady shear flow at $\dot{\gamma}$ = 0.5 s^{-1} for PSHQ9 at 130°C: experimental data are shown by dots and simulated curves by dashed lines. σ_0 and $N_{1,0}$ are the steady shear stress and first normal stress difference just prior to flow cessation.

As the shear rate increases from $\dot{\gamma}$ = 0.5 to 1.0 s^{-1}, as indicated in Figure 18, the relaxation rate of shear stress and first normal stress difference is getting a little slower.

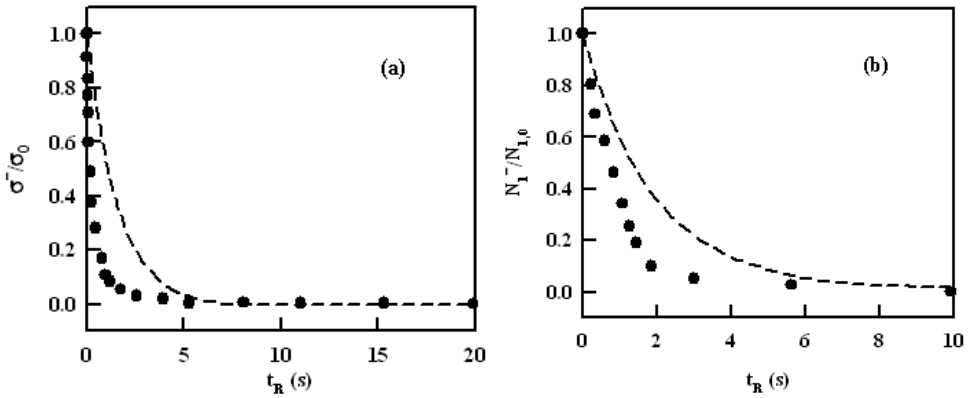

Figure 18: Relaxation of normalized (a) shear stress $\sigma^-(t)/\sigma_0$ and (b) first normal stress difference $N_1^-(t)/N_{1,0}$ upon cessation of steady shear flow at $\dot{\gamma}$ = 1 s^{-1} for PSHQ9 at 130°C: notations are the same as in Figure 17.

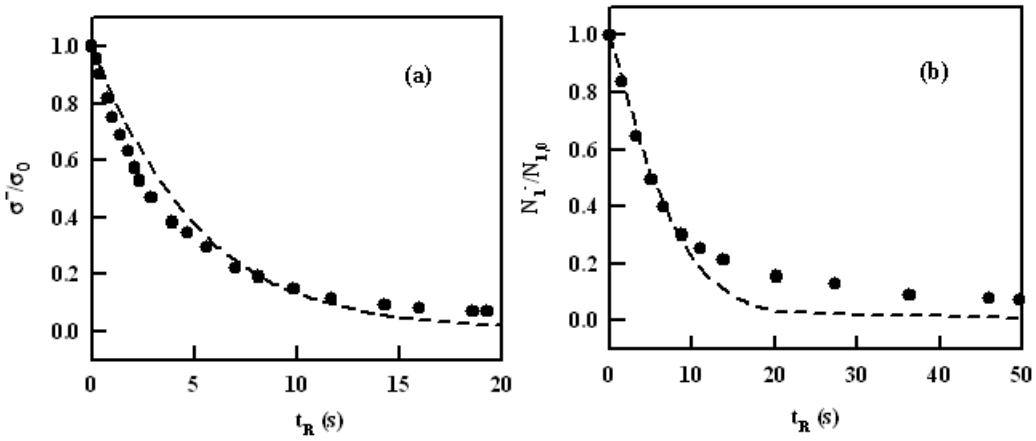

Figure 19: Relaxation of normalized (a) shear stress, $\sigma^-(t)/\sigma_0$ and (b) first normal stress difference, $N_1^-(t)/N_{1,0}$ upon cessation of steady shear flow at $\dot{\gamma}$ = 0.5 s^{-1} for PI-14-5CN at 70°C: notations are the same as in Figure 17.

Figure 19 demonstrates the relaxation of (a) normalized shear stress and (b) the first normal stress difference upon cessation of steady shear flow at $\dot{\gamma}$ = 0.5 s^{-1} for PI-14-5CN at 70°C. Experimental data are shown by dots and the fitting curves by dashed lines. As compared to Figure 15, the relaxation rates of shear stress and first normal stress difference are much faster for PI-14-5CN than for PSHQ9. This difference indicates how fast the recovery of the domain texture in side-chain LCP, PI-14-5CN is, after cessation of shear flow, as compared to that in main-chain LCP, PSHQ9. The 5CN-COOH grafted on the coil-like backbone of PI, forming PI-14-5CN, might be very mobile and thus would relax rather quickly upon cessation of shear flow, as compared to the mesogens that are linked directly to the polymer backbone of PSHQ9.

As expected and seen from Figure 20, the relaxation of shear and normal stresses for PI-14-5CN are getting slower as $\dot{\gamma}$ increases from 0.5 to 1.0 s^{-1}.

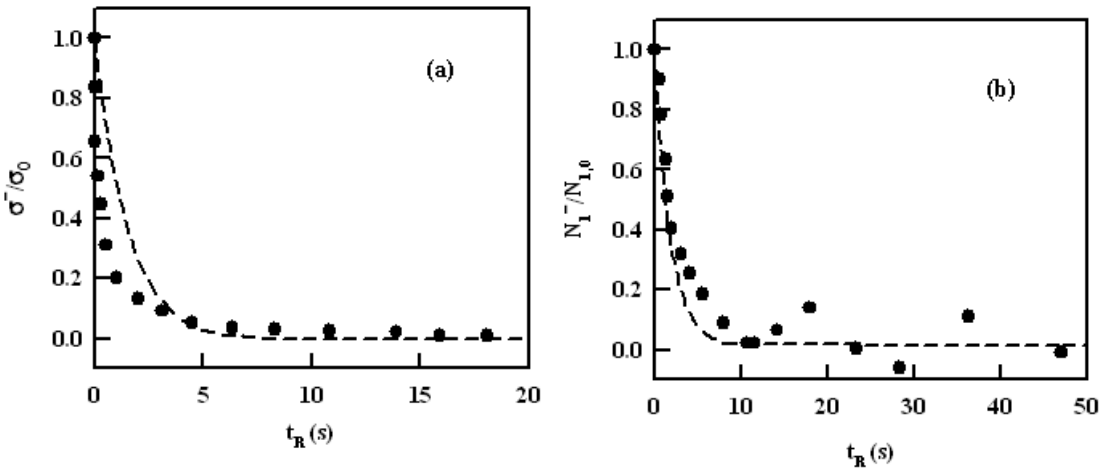

Figure 20: Relaxation of normalized (a) shear stress, $\sigma^-(t)/\sigma_0$ and (b) first normal stress difference, $N_1^-(t)/N_{1,0}$ upon cessation of steady shear flow at $\dot{\gamma}$ = 1 s^{-1} for PI-14-5CN at 70°C: notations are the same as in Figure 17.

4.4 On the Time-Temperature Superposition in Weakly Viscoelastic Nematodynamics

During the simulation of PSHQ9 and PI-14-5CN, the constitutive parameters α, β, r_1, r_2 characterizing the anisotropy of nematics, as well as the tumbling parameters λ_e, λ_v were assumed temperature independent. Thus the only two parameters, characteristic relaxation time θ_0 and viscosity η_0 were assumed changing with temperature. In this case the general equations of weak viscoelastic nematodynamics and their simple shearing specification (2) and (4) allow the scaling transformation:

$$\sigma_{ij} \to \hat{\sigma}_{ij} = \sigma_{ij}\theta_0/\eta_0, \quad t \to \hat{t} = t/\theta_0, \quad \dot{\gamma} \to \hat{\dot{\gamma}} = \dot{\gamma}\theta_0 \tag{10}$$

The transformation **(10)** demonstrates the time-temperature superposition scaling. Indeed, when the non-dimensional variables denoted in (10) by overcaps are introduced in equations **(1)** and **(2)** or in **(4)** and **(5)**, these equations will describe isothermal, generally non-steady shearing for various constant temperatures as temperature independent curves. This is the time-temperature superposition principle for weak viscoelastic nematodynamics. Because in our modeling the fitted parameters of anisotropy were temperature independent, the time-temperature superposition principle does not need to be specially checked. There are no fundamental arguments, however, why it should be valid.

5. Conclusions and Discussions

The objective of this work was to analytically and numerically describe the rheological properties of thermotropic LCP's using recently developed thermodynamic monodomain theory of weakly viscoelastic nematodynamics [22, 23] and simulate the steady and unsteady shearing data. Currently available theory by Leslie-Ericksen developed for low molecular weight liquid crystals, and Doi theory for lyotropic LCP's are not suitable for description of flow properties of thermotropic LCP's. Therefore, with the use of these theories is difficult, if possible, to predict the rheological behaviors of LCP's in general. In contrast, viscoelastic nematodynamics proposes a new general approach to circumvent this problem. It should also be noted that in spite of large number of constitutive equations proposed for many years for LCP, no attempt for simulations of

non-steady shearing has been proposed for any type of LCP's. Moreover, no theory existed up to date which could be able to describe the complicated behavior of thermotropic LCP.

In the absence of magnetic field, the theory exhibits viscoelastic transversally anisotropic behavior with symmetric stress tensor and orientation of director caused only by flow. Thus, this simplified approach has led to a closed set of two coupled anisotropic viscoelastic equations of quasi-linear type for evolution of director and extra stress; the anisotropic properties in the set being described by viscoelastic evolution equation for director. Although this theory has been developed for low enough value of Deborah number, it is still possible to compare the simulations with experimental data.

Eight parameters are involved in the theory. They are 3 viscosities, 3 elastic module, and 2 tumbling (elastic and viscous) parameters. These constitutive parameters established for steady shearing were used for the calculations of evolution of shear stress and first normal stress difference with corresponding evolution of director, during relaxation and start up flow. The problem with initial conditions for director in start up flow is resolved in the following way. We preliminarily fitted the experimental data for stresses in steady shearing with following adjustment of parameters for describing also the relaxation of stresses. In this case the parameters of evolution equation for director, along with its orientation in steady shearing were also established. The orientation of director during stress relaxation was then easily calculated, and its final orientation at the rest state was taken as initial value of director for the start up flow.

The rheological shearing data for steady and transient shear flows, and relaxation after cessation of shear flow were chosen for two industrial LCP's, Titan and Zenite 6000, as well as for two model LCP's, a main-chain LCP (PSHQ9) and a side-chain LCP (PI-14-5CN). This choice is justified by the most carefully made rheological measurements and their completeness. Specifically, Titan is random copolyester of ethylene-terephthalate (PET) and hydroxybenzoic acid (HNA) with two methylene flexible spacers, whereas Zenite 6000 is a fully aromatic copolyester with kinks, Zenite 6000 is much more rigid than Titan. The absence of region I in the apparent shear viscosity plots might be due to the fact that PI-14-5CN is a side-chain LCP, and its nematic properties might not be sufficiently strong. The mesogens in the main-chain LCP PSHQ9 are directly linked to the polymer backbone, making motions of the mesogens and backbone of PSHQ9 strongly coupled during shear flow.

The most egregious deviations of our simulations from experimental data are observed for transitional start up shearing flows. There might be several reasons for that.

The first is the weak viscoelasticity approach employed in the theory. For common polymers with long flexible chains, the weak viscoelasticity simply means the smallness of the Deborah number, $De = \theta\dot{\gamma} < 1$ where θ is the relaxation time averaged over the relaxation spectrum. In case of anisotropic LCP's where at least two relaxation times exist, the definition of Deborah number is not clear.

The second is the way of how the fitting procedure was utilized in this paper. We remind that the eight parameters were fitted to describe well enough the steady shearing data with adjusting for relaxations, for both the shear and normal stresses and for each of four LCP's of different types. We use for fitting an exhausted computerized procedure of trials and attempts. Yet, we could not find the objective criterion for the quality of this fitting procedure.

The third and perhaps the more physically feasible reason for the deviations, is the inadequacy between the theory and tested materials (or experimental procedures) selected for simulations. Yet we should state that the materials and the experimental data chosen present the best choice selected from a big pool of data. Simply, the better data do not currently exist.

The problem with start up simulations of industrial LCP's Titan and Zenith 6000 is rather procedural. In order to obtain reliable data under relatively short operational time constraint (totally about 15minutes)

preventing the samples from chemical degradation, a high level pre-shearing procedure has been used [49]. Right after short relaxation period, the rheological measurements have started, which include transient start up flow, steady shearing and relaxation from the steady shearing level. To repeat the experiments, a fresh sample should be used. Using this procedure the data showed to be reproducible. The problem with this procedure is that pre-shearing steady flow with following relaxation was not properly recorded. So our way of establishing initial value n_{1r} of director in start up flow is questionable for those materials.

Even worse, the complicated problem of polydomain behavior of model LCP's, PSHQ9 and PI-14-5CN, used in paper [54] cannot make reliable our simulations. Simply speaking, the monodomain theory we used is generally not suitable for the description of polydomain model LCP's. The polydomain effects are especially pronounced at the initial stage of start up flow, when the texture existed at rest is destroying by the growing stresses. Because this initial stage may take a lot of time, developing the steady flow might be much longer than for the monodomain case. Additionally, the procedure of finding initial value for director, established in our simulations, has no much sense in the polydomain case. On the other hand, in strong enough steady shearing flows and relaxation after their cessation, the polydomain effects are mostly insignificant. That is perhaps why the steady shearing and main relaxation processes (up to beginning the texture formation) have been well simulated using our monodomain approach. It is difficult to evaluate these effects without a good theory, which currently does not exist. So the polydomain extension of the theory has to be developed to properly describe these data. Another way to rectify this problem is to prepare the monodomain samples. Although this is feasible, it needs a lot of experimental effort.

Nevertheless, with all of these shortcomings, the simulations have demonstrated that these are at least in a semi-quantitative agreement with the chosen experimental data. Moreover, it has been found that the simulations of various LCP were in accord with their different structural features.

References

1. Chandrasekhar, S., *Liquid Crystals*, Second Ed., Cambridge University Press, **1992**.
2. de Gennes, P.G. and Prost, J., *The Physics of Liquid Crystals*, Second Ed., Clarendon Press, Oxford, **199**3.
3. Warner, M. and Terentjev, E.M., *Liquid Crystal Elastomers*, Clarendon Press, Oxford, **2003**.
4. I. Dierking, *Textures of Liquid Crystals*. Wiley-VCH: Weinheim, **2003.**
5. Larson, R.G., *The Structure and Rheology of Complex Fluids*, Oxford Press, New York **1999**.
6. P.G. Collings, M. Hird, *Introduction to Liquid Crystals Chemistry and Physics*. Taylor and Francis, London, **1997.**
7. A.M. Donald, A.H. Windle, *Liquid Crystalline Polymers*, A.M. Donald and A.H. Windle, Ed., University Press, Cambridge, **1992.**
8. de Gennes, P.G., *Mol. Cryst., Liquid Cryst*., **19**71, *12*, 193.
9. Doi M., *Molecular Theory for the Nonlinear Viscoelasticity of Polymeric Liquid Crystals*/ J.L. Ericksen, D. Kinderlehrer Eds., IMA v.5 in "Theory and Applications of Liquid Crystals", Springer-Verlag, N.Y., **1987.**
10. Larson, R.G. and Mead, D.W., *J. Rheol*. **1989**, *33*, 185.
11. Doi, M. and Edwards, S.F., *The Theory of Polymer Dynamics*, Clarendon Press, Oxford Chs.8-10, **1986**.
12. Volkov, V.S. and Kulichikhin, V.G., *J. Rheol*., **1990**, *34*, 281.
13. Pleiner, H. and Brand, H.R., *Mol. Cryst. Liq. Cryst*., **1991,** *1991*, 407.
14. Pleiner, H. and Brand, H.R., *Macromolecules*, **1992**, *25*, 895.
15. Rey, A.D., *J. Non-Newt. Fluid. Mech*., **1995**, *58*, 131.
16. Rey, A.D., *Rheol. Acta*, **1995**, *34*, 119.
17. Terentjev, E.M. and Warner, M., *Eur. Phys. J*., **2001**, *E. 4*, 343.
18. Fradkin, L.J.; Kamotski, I.V.; Terentjev, E.M. and Zakharov, D.D., *Proc. R. Soc., Lond.*, **2003**, *A 459***,** 2627.

19. Leonov, A.I. and Volkov, V.S., **2002**, *e-print: cond.mat*/0203265.
20. Leonov, A.I. and Volkov, V.S., **2003**, *e-print: cond.mat*/0202275.
21. Leonov, A.I. and Volkov, V.S., *J. Eng. Phys. Thermophys*., **2003**, *76*, 498.
22. A.I. Leonov, *J. Math. Phys. Anal. Geom.*(MPAG), **2008,** *11*, 87-116.
23. A.I. Leonov, *Zeitschr. Angew. Math. Phys*., **2008**, *59*, 333-359.
24. Marrucci, G. and Greco, F., *Adv. Chem. Phys*., **199**3, *86*, 331.
25. Feng, J.J.; Sgalari, G; and Leal, L.G. *J. Rheol.*, **2000**, *44*, 1085.
26. Edwards, B.J.; Beris, A.N. and Grmela, M., *J. Non-Newt Fluid Mech*., **199**0, *35*, 51.
27. Beris, A.N. and Edwards, B.J., *Thermodynamics of Flowing Systems*, Oxford University Press, Oxford, **1999**.
28. Volkov,V.S. and Kulichikhin, V.G., *Macromolec. Symposia, Statistical Mechanics of Polymers*, **1994,** *81***,** 45.
29. Long, D. and Morse, D.C., *J. Rheol.* , **2002**, *46*, 49.
30. Pickett, G.T. and Schweizer, K.S., *J. Chem. Phys*., **2000**, *112*, 4869.
31. Pickett, G.T. and Schweizer, K.S., *J. Chem. Phys*., **2000**, *112*, 4881.
32. L. Golubovich, L. and Lubensky, T.C., *Phys. Rev. Lett.*,**1989**, *63*, 1082.
33. Olmsted, P.D., *J. Phys.II France*, **1994**, *4*, 2215.
34. Lubensky, T.C. and R. Mukhopadya, R., *Phys. Rev.E*, **2002**, 66, 011702.
35. Leonov, A.I. and Volkov, V.S., *J. Engn. Phys. and Thermophys*, **2004**, *77*, 717.
36. Leonov, A.I. and Volkov, V.S., *Rheol. Acta* , **2005**, *44*, 331.
37. de Gennes, P.G., in: *Liquid Crystals in One- and Two Dimensional Order*, ed, W. Helfrich & G. Kleppke, Springer, Berlin, **1980,** pp. 231-237.
38. Leonov, A.I., *Rheol. Acta*, **2005**, *44***,** 573.
39. Odell, P.A., Unger,G. and Feijo, J.L., *J. Polym. Sci.: Polym. Phys*., **1993**, *31*, 141.
40. Yang, X., Forest, M.G.., Mullins, W., and Wang, Q., *J. Rheol*., 2009, *53*, 589.
41. Ericksen, J.L., *Arch. Rat. Mech. Anal*., **1991**, *113*, 97.
42. Guenther, G.K.; Baird, D.G. and Davis, R.M., in: *Liquid Crystalline Polymers*, Proceedings of the International Workshop on Liquid Crystalline Polymers, WLCP'93, Capri, Italy, June 1-4, 1993, C. Carfagne, Ed., New York, Elsevier, **1994**, pp. 133-142.
43. Einaga, Y.; Berry G.C. and Chu, S.-G., *Polymer (Japan)*, **1985**, *17*, 239.
44. Ernst, B. and Denn, M.M., *J. Rheol*., **1992**, *36*, 289.
45. Han, C.D. and Kim, S.S., *Macromolecules*, **1993,** *26*, 3176.
46. Kim, S.S. and Han, C.D., *Macromolecules*, **1993**, *26*, 6633.
47. Ugaz, V.M. and Burghardt, W.R., *Macromolecules*, **1998**, *31*, 8474.
48. Han, C.D.; Ugaz, V.M. and Burghardt, W.R, *Macromolecules*, **2001**, *34*, 3642.
49. Belatreche, M. J., *An Experimental and Theoretical Study of Liquid Crystal Polymers*, M.S. Thesis, The University of Akron, Akron, OH, 2002.
50. Onogi, T. A., in: *Proceedings of the Seventh International Congress on Rheology*. Astarita, G., Marrucci, G. and Nicolais, L., Eds.; Plenum Press: New York, **1980**, Vol I, pp 127.
51. Marrucci, G. and Maffettone, P.L., *J. Rheol.* **1990,** *34*, 1217-30.
52. Larson R.G. and Doi, M., *J. Rheol.* **1991**, *35*, 539-63.
53. Han, C.D., *Rheology and Processing of Polymeric Materials*. Oxford University Press, New York, Vol. I, **2007.**
54. Lee K.M. and Han, C.D., *Macromolecules* **2002**, *35*, 6263-73.